5. DeGrado TR, Holden JE, Ng CK, Raffel DM, Gatley SJ. β-Methyl-15-p-iodophenylpentadecanoic acid metabolism and kinetics in the isolated rat heart. *Eur J Nucl Med* 1989;15:78–80.
6. DeGrado TR. Synthesis of 14(R,S)-[^{18}F]fluoro-6-thia-heptadecanoic acid (FTHA). *J Labeled Comp Radiopharm* 1991;29:989–995.
7. Skrede S, Narce M, Bergseth S, Bremer J. The effects of alkylthioacetic acids (3-thia fatty acid) on fatty acid metabolism in isolated hepatocytes. *Biochim Biophys Acta* 1989;1005:296–302.
8. DeGrado TR, Coenen HH, Stocklin G. 14(R,S)-[^{18}F]fluoro-6-thia-heptadecanoic acid (FTHA): evaluation in mouse of a new probe of myocardial utilization of long chain fatty acids. *J Nucl Med* 1991;32:1888–1896.
9. Patlak CS, Blasberg RG, Fenstermacher JD. Graphical evaluation of blood-to-brain transfer constants from multiple-time uptake data. *J Cereb Blood Flow Metab* 1983;3:1–7.
10. Nickles RJ, Gatley SJ, Votaw JR, Kornguth ML. Production of reactive fluorine-18. *Int J Radiat Appl Instrum Part A* 1986;37:649–661.
11. Liedtke AJ, Renstrom B, Nellis SH. Correlation between [5-^{3}H]glucose and [U-^{14}C]deoxyglucose as markers of glycolysis in reperfused myocardium. *Circ Res* 1992;71:689–700.
12. Renstrom B, Nellis SH, Liedtke AJ. Metabolic oxidation of glucose during early myocardial reperfusion. *Circ Res* 1989;65:1094–1101.
13. Liedtke AJ, DeMaison L, Eggleston AE, Cohen LM, Nellis SH. Changes in substrate metabolism and effects of excess fatty acids in reperfused myocardium. *Circ Res* 1988;62:535–542.
14. Renstrom B, Nellis SH, Liedtke AJ. Metabolic oxidation of pyruvate and lactate during early myocardial reperfusion. *Circ Res* 1990;66:282–288.
15. Nellis SH, Liedtke AJ, Renstrom B. Distribution of carbon flux within fatty acid utilization during myocardial ischemia and reperfusion. *Circ Res* 1991;69:779–790.
16. Rose CP, Goresky CA. Constraints on the uptake of labeled palmitate by the heart. The barriers at the capillary and sarcolemmal surfaces and the control of intracellular sequestration. *Circ Res* 1977;41:534–545.
17. Saddik M, Lopaschuk G. Myocardial triglyceride turnover during reperfusion of isolated rat hearts subjected to a transient period of global ischemia. *J Biol Chem* 1992;267:3825–3831.
18. Abu-Erreish GM, Neely JR, Whitmer JT, Whitman V, Sanadi DR. Fatty acid oxidation by isolated perfused working hearts of aged rats. *Am J Physiol* 1977;232:E258–E262.
19. Hamilton JG, Comai K. Rapid separation of neutral lipids, free fatty acids and polar lipids using prepacked silica Sep-Pak columns. *Lipids* 1988;23:1146–1149.
20. Pooley RA. Evaluation of 14(R,S)[fluorine-18]fluoro-6-thia-heptadecanoic acid (FTHA) as a positron emission tomography fatty acid tracer of β-oxidation in the heart. [PhD thesis]. Madison, WI: University of Wisconsin-Madison; 1995.
21. Gandemer GG, Durand G, Pascal G. Relative contribution of the main tissues and organs to body fatty acid synthesis in the rat. *Lipids* 1983;18:223–228.
22. Van der Vusse GJ, Roemen THM, Flameng W, Reneman RS. Serum myocardium gradients of nonesterified fatty acids in the dog, rat and man. *Biochem Biophys Acta* 1983;752:361–370.
23. Veerkamp JH, Van Moerkerk HTB, Glatz JFC, Zuurveld JGEM, Jacobs AEM, Wagenmakers AJM. $^{14}CO_2$ production is no adequate measure of [^{14}C]fatty acid oxidation. *Biochem Med Metab Biol* 1986;35:248–259.
24. Sherratt HSA, Watmough NJ, Johnson MA, Turnbull DM. Methods for study of normal and abnormal skeletal muscle mitochondria. *Methods Biochem Anal* 1988;33:243–335.
25. Kler RS, Sherratt HSA, Turnbull DM. The measurement of mitochondrial β-oxidation by release of $^{3}H_2O$ from [9,10-^{3}H]hexadecanoate: application to skeletal muscle and the use of inhibitors as models of metabolic disease. *Biochem Med Metab Biol* 1992;47:145–156.
26. Lerch RA, Ambos HD, Bergmann SR, Sobel BE, Ter-Pogossian MM, Sobel BE. Effect of flow-independent reduction of metabolism on regional myocardial clearance of ^{11}C-palmitate. *Circulation* 1982;65:731–738.
27. Grover-McKay M, Schelbert HR, Schwaiger M, et al. Identification of impaired metabolic reserve by atrial pacing in patients with significant coronary artery stenosis. *Circulation* 1986;74:281–292.
28. Hansen CL, Jeo J, Oliner C, Van Decker W, Iskandrian AS. Prediction of improvement in left ventricular function with iodine-123-IPPA after coronary revascularization. *J Nucl Med* 1995;36:1987–1993.
29. Goodman MM, Knapp FF Jr, Callahan AP, Ferren LA. A new well-retained myocardial imaging agent: radioiodinated 15-(p-iodophenyl)-6-tellurapentadecanoic acid. *J Nucl Med* 1982;23:904–908.
30. Fagret D, Bontemps L, Apparu M, et al. Kinetics of iodomethylated hexadecanoic acid metabolism in the rat myocardium: influence of the number and the position of methyl radicals. *Int J Nucl Med Biol* 1985;12:363–367.
31. Chouraqui P, Maddahi J, Henkin R, Karesh SM, Galie E, Berman DS. Comparison of myocardial imaging with iodine-123-iodophenyl-9-methyl pentadecanoic acid and thallium-201-chloride for assessment of patients with exercise-induced myocardial ischemia. *J Nucl Med* 1991;32:447–452.
32. Sloof GW, Visser FC, Eenige van MJ, et al. Comparison of uptake, oxidation and lipid distribution of 17-iodoheptadecanoic acid, 15-(p-iodophenyl)pentadecanoic acid and 15-(p-iodophenyl)-3,3-dimethylpentadecanoic acid in normal canine myocardium. *J Nucl Med* 1993;34:649–657.
33. Knapp FF, Ambrose KR, Goodman MM. New radioiodinated methyl-branched fatty acids for cardiac studies. *Eur J Nucl Med* 1986;12(suppl):S39–S44.
34. Nishimura T, Sago M, Kihara K, et al. Fatty acid myocardial imaging using ^{123}I-beta-methyl-iodophenyl pentadecanoic acid (BMIPP): comparison of myocardial perfusion and fatty acid utilization in canine myocardial infarction (occlusion and reperfusion model). *Eur J Nucl Med* 1989;15:341–345.
35. Bianco JA, Pape LA, Alpert JS, et al. Accumulation of radioiodinated 15-(p-iodophenyl)-6-tellurapentadecanoic acid in ischemic myocardium during acute coronary occlusion and reperfusion. *J Am Coll Cardiol* 1984;4:80–87.
36. Poe ND, Robinson GD, Graham SL, MacDonald NS. Experimental basis for myocardial imaging with ^{123}I-labeled hexadecanoic acid. *J Nucl Med* 1977;17:1077–1082.
37. Geltman EM, Smith JL, Beecher D, Ludbrook PA, Ter-Pogossian MM, Sobel BE. Altered regional myocardial metabolism in congestive cardiomyopathy detected by positron tomography. *Am J Med* 1983;74:773–785.
38. Eisenberg JD, Sobel BE, Geltman EM. Differentiation of ischemic from nonischemic cardiomyopathy with positron emission tomography. *Am J Cardiol* 1987;59:1410–1414.

Generation of Myocardial Factor Images Directly from the Dynamic Oxygen-15-Water Scan Without Use of an Oxygen-15-Carbon Monoxide Blood-Pool Scan

Flemming Hermansen, John Ashburner, Terry J. Spinks, Jaspal S. Kooner, Paolo G. Camici and Adriaan A. Lammertsma

PET Methodology and Cardiology Groups, Cyclotron Unit, MRC Clinical Sciences Centre, Hammersmith Hospital, London; and Department of Cardiology, Royal Postgraduate Medical School, Hammersmith Hospital, London, United Kingdom

The measurement of regional myocardial blood flow (MBF) with $H_2{}^{15}O$ and PET requires an additional $C^{15}O$ blood-pool scan for the purpose of region of interest (ROI) definition. This additional scan results in a substantially increased radiation dose, study duration and risk of movement artifacts. Therefore, a method was developed to generate myocardial factor images directly from the dynamic $H_2{}^{15}O$ study without the need for a $C^{15}O$ scan. **Methods:** The factor sinograms were generated by means of linear dimension reduction of the dynamic sinograms, where the required variate and covariate factors (myocardial and blood time-activity curves) were modeled from the lung time-activity curve. The factor images were generated by iterative reconstruction. **Results:** No significant difference was found between MBF values from ROIs drawn on the traditional images (using the $C^{15}O$ scan) and those drawn on the factor images. **Conclusion:** It is possible to generate myocardial images directly from the dynamic $H_2{}^{15}O$ study, so that the $C^{15}O$ scan can be omitted from MBF studies. The proposed method is robust and results in nearly optimal signal-to-noise ratios in the factor images.

Key Words: PET; myocardial blood flow; factor analysis; myocardial and blood-pool images

J Nucl Med 1998; 39:1696–1702

The measurement of regional myocardial blood flow (MBF) with $H_2{}^{15}O$ and PET is an established technique based on the favorable properties of $H_2{}^{15}O$ as a flow tracer (*1–3*). The main

Received Jan. 9, 1997; revision accepted Jan. 14, 1998.

For correspondence or reprints contact: Flemming Hermansen, MD, PET Center, Aarhus General Hospital, 44 Norrebrogade, Aarhus C, Denmark DK-8000.

Present address: Adriaan A. Lammertsma, PhD, PET Centre, Free University Hospital, Amsterdam, The Netherlands.

drawback of $H_2{}^{15}O$ is the lack of a myocardial image suitable for region of interest (ROI) definition, due to the similar concentrations in arterial blood and myocardial tissue. Therefore, an image of the myocardium is often generated by performing an additional $C^{15}O$ scan and subtracting the corresponding blood volume image from either a transmission density image (*4*) or an image of the washout phase of the dynamic $H_2{}^{15}O$ scan (*2*). There are, however, several disadvantages associated with this additional $C^{15}O$ scan: (a) the subtraction images are very sensitive to patient movement between scans, possibly resulting in mispositioning of ROIs; (b) special hardware is required to generate and safely deliver the $C^{15}O$ gas; (c) there is a substantial increase in radiation dose to the patient; and (d) the total study duration increases by about 15 min, thereby enhancing the risk of patient movement.

Ideally, the myocardial and blood-pool images should be generated from the dynamic $H_2{}^{15}O$ scan itself without the need for an additional $C^{15}O$ scan. However, since these dynamic images contain a considerable amount of noise, optimal handling of signal-to-noise (S/N) ratio is crucial for generation of the myocardial and blood-pool images, and no method is currently able to do this satisfactorily.

Recently, a general theory for optimal linear dimension reduction of sequences of medical images have been reported (*5,6*). The feasibility of generating myocardial images with optimal noise properties from $H_2{}^{15}O$ scans was demonstrated, but the method required left and right ventricular cavity (LVC and RVC) time-activity curves (TACs), which are difficult to obtain. The aims of this study were first to model these TACs from the lung time-activity curve for the generation of myocardial and blood-pool factor images and, second, to test whether these factor images could be used for ROI definition with the view of quantifying MBF, thereby eliminating the need for an additional $C^{15}O$ scan.

THEORY

Linear Dimension Reduction

This study is based on a simplified general theory for linear dimension reduction (*6*), which performs the dimension reduction in such a way that the noise in the resulting factor images is minimized. An initial transformation to obtain homogeneous variance is first performed. Thereafter, the variance of the noise is kept constant in all calculations by allowing attenuation of the signal. This differs from the traditional approach where the signal is calculated, but the noise is allowed to increase (*5*). The above mentioned initial transformation significantly simplifies the equations (*6*). The optimal linear dimension reductions are orthogonal projections, and the noise will be uncorrelated between any set of orthogonal coordinates. In addition, results are not degraded by subdivision of the time-intervals (*6*).

In short, the method requires that a variate factor (f_1 representing a time-activity curve for the organ that should be imaged by the factor image) and covariate factors ($f_2, \ldots, f_p$, representing TACs of other structures) are given. The pixel vectors must have been scaled appropriately (*6*). The variate factor is allowed to contain spillover from the covariate factors, but the covariate factors should not contain spillover from the variate factor. The variate and covariate factors should be supplied for each separate factor image and are specified in the modeling section later. The factor image with optimal S/N ratio is now obtained as those parts of the scaled pixel vectors that are placed in the subspace V_{pv} in the following orthogonal sum (*6*):

$$V = V_S \perp V_r = V_{pv} \perp V_c \perp V_r, \qquad \text{Eq. 1}$$

where

V = scaled data space,
V_S = span($f_1, f_2, \ldots f_p$) = the signal space,
V_c = span($f_2, \ldots f_p$) = the covariate space,
V_{pv} = the projected variate space,
V_r = the residual space and
$\perp$ denotes an orthogonal sum.

In other words, factor images with the optimal S/N ratio are obtained by first orthogonally projecting each scaled pixel vector onto the signal subspace [V_s = span($f_1, f_2, \ldots f_p$)]. The projected vectors are then further projected orthogonally onto the subspace (V_{pv} c V_s) that is orthogonal to the covariate subspace [V_c = span($f_2, \ldots f_p$)].

Equation 1 not only specifies how factor images with optimal S/N ratio should be constructed (when linear dimension reductions are used), it also provides the amplitude of the projected signals (i.e., the norm of the part of the signal vectors that are placed in V_{pv}). The variance of the noise remains unchanged after orthogonal projections, so Equation 1 also specifies the S/N ratio in the factor images, and it can be used to examine the effects of errors in the variate and covariate vectors. Further details are given elsewhere (*6*).

Modelling the Variable and Covariable Factors

Myocardial factor images can be generated by using one variate and two covariate factors (*6*):

$$\begin{aligned} V_S &= \text{span}(y_{myocardium}, y_{lvc}, y_{rvc}) \\ V_c &= \text{span}(y_{lvc}, y_{rvc}), \end{aligned} \qquad \text{Eq. 2}$$

where y_{lvc} and y_{rvc} are the scaled LVC and RVC time-activity curves and $y_{myocardium}$ is the scaled $x_{myocardium}$.

$$x_{myocardium}(t) = F \times x_{input}(t) * \exp[-(F/p + \lambda) \times t], \qquad \text{Eq. 3}$$

where

t = time [min],
$x_{myocardium}(t)$ = myocardium concentration of $H_2{}^{15}O$ [Bq ml^{-1} (tissue)],
$x_{input}(t)$ = arterial concentration of $H_2{}^{15}O$ [Bq ml^{-1} (blood)],
F = MBF [ml (blood) ml^{-1} (tissue) min^{-1}],
p = myocardium to blood partition coefficient of water [(ml water/ml tissue)/(ml water/ml blood)],
λ = decay constant of ^{15}O (= 0.338 min^{-1}) and
$*$ denotes convolution.

The partition coefficient can be set to $p = 0.96$ ml ml^{-1} (*3*). The method to generate factor images is relatively insensitive to the chosen value of F (*6*), which is set to 0.75 ml (blood) ml^{-1} (tissue) min^{-1} in this study. The LVC and RVC time-activity curves (x_{lvc} and x_{rvc}) are difficult to obtain from ROIs before the factor images have been generated so, in this study, they were modeled from the lung time-activity curve (x_{lung}). The lung curve primarily differs from the LVC and RVC curves in dispersion and delay. Therefore, the simplest model to obtain x_{lvc} and x_{rvc} is a time shift of x_{lung}:

$$\begin{aligned} x_{lvc}(t) &= x_{lung}(t - \Delta t) \\ x_{rvc}(t) &= x_{lung}(t + \Delta t) \\ x_{input}(t) &= x_{lung}(t) \end{aligned} \qquad \text{Eq. 4}$$

The effect of using $\Delta t = 10$ sec as well as $\Delta t = 5$ sec was examined in this study.

Blood factor images can also be generated by means of Equation 1 but with the role of blood and myocardium interchanged so that:

$$V_S = \text{span}(y_{\text{myocardium}}, y_{\text{lung}})$$
$$V_c = \text{span}(y_{\text{myocardium}}) \qquad \text{Eq. 5}$$

Weighting

The pixel vectors were scaled in such a way that homogeneous variance was obtained. This was achieved by assuming that the variance of the noise in a pixel vector was proportional to the total number of counts in a sinogram (*6,7*).

MATERIALS AND METHODS

Scanning Protocol

The method was developed using data previously acquired for comparison of different administration protocols of $H_2{}^{15}O$ consisting of 4 normal subjects and 11 patients with ischemic heart disease (*8*). The studies were approved by the Research Ethics Committee of Hammersmith Hospital. Permission to administer the radioactive tracers was obtained from the United Kingdom Administration of Radioactive Substances Advisory Committee. Written informed consent was obtained from all subjects before scanning.

All scans were acquired with an ECAT 931-08/12 whole-body scanner (Siemens/CTI, Knoxville, TN) with an axial field of view of 10.8 cm. Before scanning, an antecubital vein was cannulated for blood sampling and subsequent tracer administration. After positioning the subject, a rectilinear transmission scan was acquired to check that the heart was located in the center of the axial field of view of the scanner. Then a transmission scan (20 min) was acquired using retractable $^{68}Ge/^{68}Ga$ ring sources. This transmission scan was used to correct all subsequent emission scans for attenuation: (a) $C^{15}O$ blood-pool scan (6 GBq, efficiency of gas mask ~50%); (b) dynamic $C^{15}O_2$ inhalation scan (7 GBq, efficiency of gas mask ~50%); (c) dynamic $H_2{}^{15}O$ infusion scan (550-1100 MBq); and (d) dynamic $H_2{}^{15}O$ bolus scan (~550 MBq) (*8*). All scans were performed at baseline without any pharmacological intervention. The time between emission scans ranged from 15–25 min to allow for decay and data transfer. For this study, only the dynamic $H_2{}^{15}O$ bolus scan was used, together with the $C^{15}O$ blood-pool scan for validation purposes. The $H_2{}^{15}O$ scan comprised 34 frames over 7 min (1 × 30 sec background, 12 × 5 sec, 15 × 10 sec, 6 × 30 sec). Starting after the background frame, $H_2{}^{15}O$ was injected as a bolus (~550 MBq) over 20 sec with an infusion rate of 10 ml min^{-1}. Then, the line was flushed for another 2 min.

Image Processing

The normalization scan (acquisition of a flat source) was extended as previously reported (*9*) to include the arms within the normalization field of view. This scan was used to correct all other scans for inhomogeneities in the detector system.

In the flowchart of Figure 1, a schematic representation of the various processing steps (after normalization and attenuation correction) is given both when ROIs are defined, using the new factor image method, and when they are defined on blood volume, washout and extravascular density images (traditional method).

Transmission and dynamic $H_2{}^{15}O$ images were filtered backprojected using a Hann filter with a cutoff frequency of 0.5 in units of the reciprocal of the sampling interval of the projection data (3.07 mm). The resulting image resolution was 8.4 × 8.3 × 6.6 mm (*3*) FWHM, and the pixel size was 2.096 mm. Lung TACs for generation of the factor images were obtained by defining ROIs on

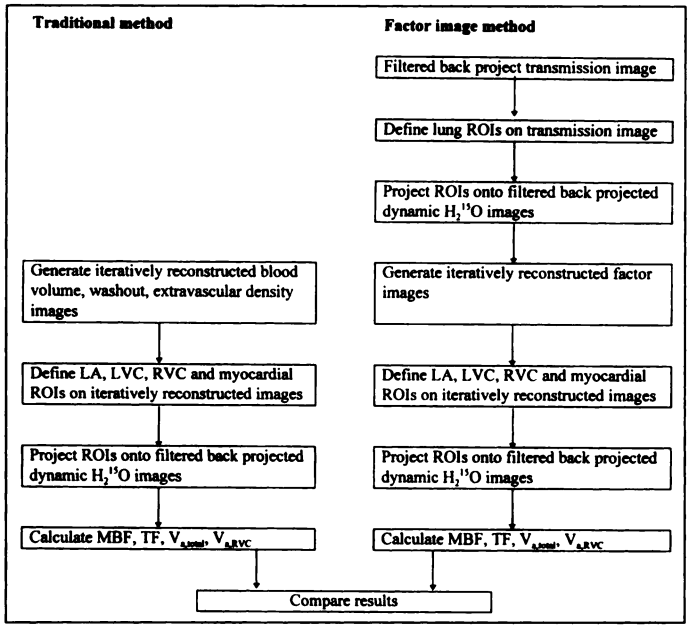

FIGURE 1. Processing steps when regions of interest (ROIs) are defined on factor images versus traditional images.

transmission images and applying them to the dynamic $H_2{}^{15}O$ filtered backprojected images. The myocardial factor images were generated using the lung curve, shifted by 10 sec in each direction ($\Delta t = 10$ sec), to represent the LVC and RVC time-activity curves, respectively. Blood volume images (*2*) (from $C^{15}O$), washout images [i.e., washout phase of $H_2{}^{15}O$ images minus appropriately scaled $C^{15}O$ image to remove the blood (*2*)], extravascular density images (*4*) and factor images were iteratively reconstructed (*10,11*) using 64 iterations with area weighted forward- and backprojections and smoothing (*12*) with the kernel (0.01, 0.98, 0.01) in the x and y directions and resliced into 12 short-axis planes. Washout and extravascular density images, which are generated as a difference between two other images, were obtained by first iteratively reconstructing these images separately before subtraction. This was necessary since the iterative reconstruction requires that all sinogram data are non-negative (*10*). This was also true for the factor images where the two sum images corresponding to the positive, and the negative factor coefficients were reconstructed separately. The resolution of the iteratively reconstructed images was 7.7 × 7.7 × 6.6 mm (*3*) FWHM.

Regions of Interest Definition to Calculate Myocardial Blood Flow

Two independent sets of ROIs were defined (see Fig. 1) on the iteratively reconstructed short-axis images. Each set consisted of left atrial (LA), LVC and RVC ROIs together with myocardial ROIs for the septum and nonseptum defined in the eight central short-axis images. LA ROIs were not defined in three of these subjects, where only part of the atrium was scanned. First, ROIs were defined in the traditional way on blood volume, washout and extravascular density images as described previously (*8*). A note was made of the short-axis plane numbers for the ROIs. The same planes were used when the second set of ROIs was defined on the blood factor and myocardial images a few weeks later by the same operator. This procedure was followed to avoid differences in the TACs, which could be attributed primarily to differences between the planes rather than to the way the ROIs were drawn within planes.

Several measures were taken to reduce variability in the defined ROIs and the corresponding TACs. The ROI definition program ensured that the thickness of the myocardial ROIs was always 6

pixels, corresponding to 12.6 mm (*8*). Because iteratively reconstructed images had higher resolution than the corresponding filtered backprojected images, blood ROIs were always defined such that a safe distance was kept from myocardial tissue (to avoid spillover). LVC ROIs were defined by keeping a safe distance from especially the lateral wall (which moves most) and the papillary muscles. RVC ROIs were defined, keeping a safe distance from the septum.

To obtain quantitative TACs, all ROIs were then projected onto the filtered backprojected dynamic images.

Data Analysis

A traditional single-tissue compartment model was used for calculating the tissue time-activity curve from the LVC input curve and MBF. The LVC and RVC TACs from both sets of ROIs (i.e., traditional method and factor image method, see Fig. 1) were used in weighted (to achieve homogeneous variance of the noise in each point) nonlinear regression to fit for MBF, tissue fraction (TF), spillover of blood from the LVC into the myocardium ($V_{a,lvc}$) and, in the septum, the separate spillover from the RVC into myocardium ($V_{a,rvc}$). This is the traditional (3-parameter model) method (*2,3*), except that it contains two spillover terms (4-parameter model), when applied to the septum (*8*). $V_{a,total}$ is defined as $V_{a,lvc} + V_{a,rvc}$.

These calculations were performed with the LA TACs, as well as the LVC TACs, as input curves. The results from both sets of ROIs were compared to assess whether factor images could be used instead of traditional images.

The impact of the modeling (of variate and covariate spaces) on the S/N ratio in the myocardial factor images was examined. The generation of myocardial images assumes that the myocardial blood flow equals 0.75 ml min^{-1} ml^{-1}. Using the lung time-activity curve as input function, the S/N ratio was calculated for different myocardial blood flows using Equations 1 and 3. In practice, the true input function is a delayed and dispersed version of the lung time-activity curve. Therefore, the true myocardial time-activity curve will also be a delayed and dispersed version of the calculated (using Eq. 3) myocardial curve. To assess the effect of this (in practice unknown) delay and dispersion from the lungs to the coronary arteries on the S/N ratio, the S/N ratio of the myocardium was also calculated after delaying the calculated myocardial curve by 5 sec and 10 sec. Assuming that the RVC and LVC TACs are correct, the residual blood in the myocardial images was calculated with Equation 1. The above calculations were performed for both $\Delta t = 5$ sec and $\Delta t = 10$ sec (for elimination of blood in the factor images) in Equation 4. Detailed equations for performing the above calculations are given in (*6*).

RESULTS

The average pixel ROI sizes for LA, LVC and RVC were 66 (*62*), 59 (*56*) and 68 (*61*), respectively, when drawn on factor (traditional) images.

Figure 2 shows iteratively reconstructed myocardial and blood factor images together with the traditional $C^{15}O$ blood volume, washout and extravascular density images. As a result of the approximations in modeling $x_{lvc}(t)$ and $x_{rvc}(t)$, the cavities in the myocardial factor images are not exactly zero, but on average slightly negative. Since the purpose was to obtain factor images with optimal S/N ratios for the purpose of ROI definition, no attempts were made to ensure that the blood in the right and left ventricular cavities was scaled in the same way in the blood factor images. Usually, the amplitude of the blood in the RVC was higher than that in the LVC.

Table 1 shows average differences (± s.d.) of the fitted parameters when the ROIs were defined on the factor images

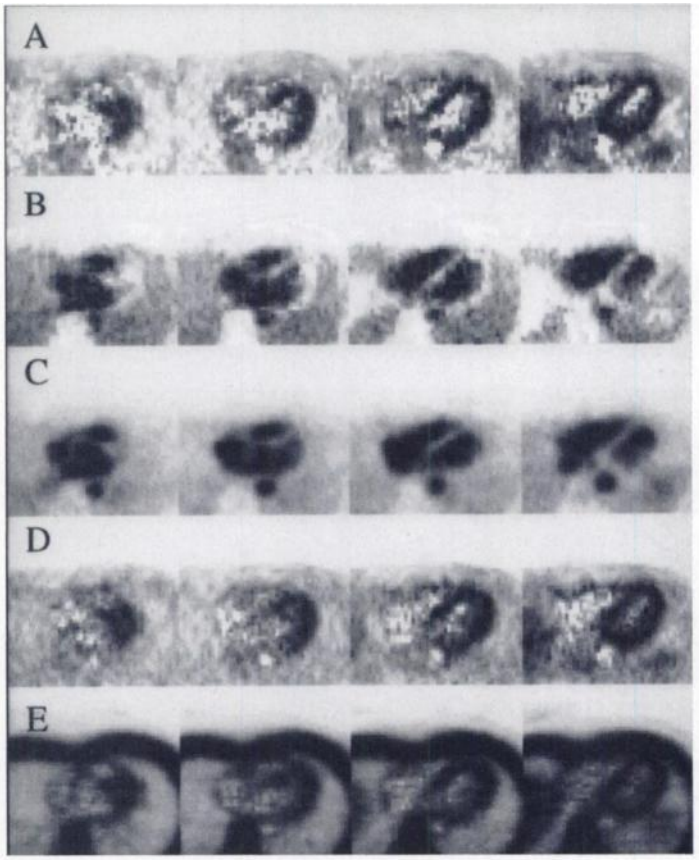

FIGURE 2. Myocardial and blood factor images. Transaxial views of factor images of (A) myocardium and (B) blood and of (C) traditional $C^{15}O$ blood-volume, (D) washout and (E) extravascular density images. All images have been iteratively reconstructed.

when compared with the traditional images (washout, extravascular and $C^{15}O$ blood volume images). The differences were small, although some were statistically significant.

Table 2 shows the retrieval of signals in the myocardial factor images (i.e., the proportional rms magnitude of the original scaled signal that is found in the myocardial factor image). The retrieval of the myocardium (with MBF = 0.75 ml min^{-1} ml^{-1}) varies from 0.57–0.65 (0.61–0.69) depending on the actual average delay from 0 sec to 10 sec between the lung and the coronary artery time-activity curves when modeling the covariates (Eq. 4) using $\Delta t = 10$ sec ($\Delta t = 5$ sec). In other words, a change in average delay causes a change in recovery (and hence in S/N ratio) of 1.2% per second. The retrieval of the measured LVC and RVC time-activity curves was, on average (15 subjects), slightly negative (−0.01 to −0.05) with a s.d. of 0.05. Since these TACs possibly contain some spillover of myocardial activity (which has positive retrieval), the true retrieval of blood is probably slightly more negative.

Figure 3 shows the amplitude of the myocardium in the myocardial factor image as a function of the true MBF. The amplitude is also proportional to the S/N ratio. The lung curve (with no delay) was used as an input function for calculating the myocardial signal. The total signal represents S/N ratio of an optimally weighted summed image. The total signal − covariates represents the S/N ratio of myocardium after the covariates (modeled using $\Delta t = 5$ sec) have been removed. This represents the signal that can be retrieved if the MBF of the variate vector ($x_{myocardium}$) is adjusted to match the true MBF. The projected variate is the signal that is actually retrieved when using MBF = 0.75 ml min^{-1} ml^{-1} for the variate vector. Over the MBF range from 0.17–2.00 ml min^{-1} ml^{-1}, the additional loss

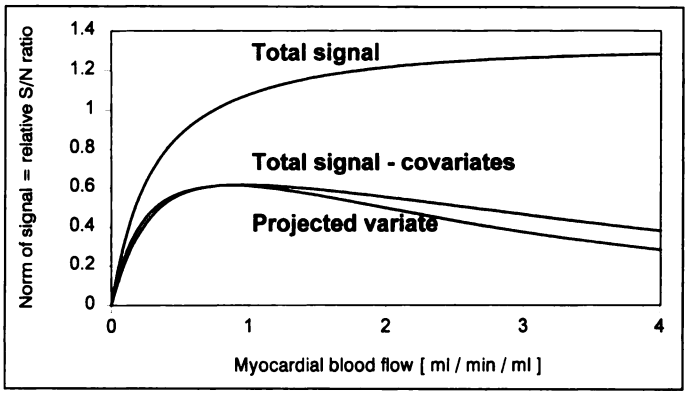

FIGURE 3. Signal-to-noise (S/N) ratios in myocardial factor images. Relative amplitude (=relative S/N ratio) in myocardium as function of myocardial blood flow (MBF) in optimally weighted summed image (total signal) and after removal of blood using both matched flow model (total signal−covariates) and fixed-flow model (MBF = 0.75 ml min^{-1} ml^{-1}) of this study (projected variate). Scale has been chosen so that MBF = 0.75 ml min^{-1} ml^{-1} has relative S/N ratio = 1.

in S/N ratio as a result of using a fixed value of MBF (=0.75 ml min^{-1} ml^{-1}) was less than 10%. At MBF = 4 ml min^{-1} ml^{-1}, the additional loss was 26%. The retrieval of both the projected variate and the total signal − covariates was somewhat lower for hyperemic MBF values when Δt = 10 sec was used in modeling the covariates, indicating that Δt = 5s results in lower noise in the myocardial factor image than Δt = 10 sec.

DISCUSSION

The main result of this study is a robust method for generating myocardial and blood factor images directly from dynamic $H_2{}^{15}O$ scans, so that ROIs can be defined for the calculation of MBF without the need for an additional $C^{15}O$ scan. The proposed method simplifies the measurement of MBF with $H_2{}^{15}O$, thereby adding to the favorable properties of $H_2{}^{15}O$ as a flow tracer (*3*). Importantly, the study can be repeated after only 10–15 min, and the calculated MBF values are independent of the actual partial volume.

The proposed method uses blood and myocardial factor images generated from the dynamic $H_2{}^{15}O$ scan itself. This eliminates the problem of patient movement between scans, enabling a more accurate definition of ROIs. The myocardial factor images in Figure 2 show a small oversubtraction of the blood pool. This is a general tendency (Table 2) caused by the simplified modeling of the RVC and LVC TACs using the lung curve. This oversubtraction, though small, might affect the definition of the myocardial ring-shaped ROIs. It has been shown (*3,13*) that the size and placement of ROIs may affect the calculated MBF, TF and $V_{a,total}$ values. This effect is minor, however, because the model fits for partial volume and spillover. The width of the ROIs (1.26 cm) is a compromise between obtaining a high S/N ratio versus a high-tissue fraction and a low spillover (*3*). Table 1 shows small, but significant, differences in TF and $V_{a,total}$, which may be attributed to differences in placement of the ROIs, in particular the difference in size. It is, however, important to notice that the same MBF values are obtained when ROIs are drawn on the factor images and on the traditional images.

In general, it was easy to define the LVC ROIs on the myocardial factor images. In particular, the direct visualization of the myocardial wall and myocardial spillover was useful. Definition of LA ROIs was, however, difficult in some of the patients because it requires more anatomical knowledge, and the blood factor images contain more noise than the $C^{15}O$ blood volume images. This is due to several reasons. First, the $C^{15}O$ activity was higher than the $H_2{}^{15}O$ activity. Second, $C^{15}O$ is confined to the blood space, whereas $H_2{}^{15}O$ distributes over the entire water space. Third, the partitioning of the dynamic $H_2{}^{15}O$ scan into myocardial and blood factor images further attenuates the images. LA ROIs can, however, be replaced by LVC ROIs since these give, in practice, the same average MBF values (*3,8,13*).

The present theory allows for calculation of relative S/N ratios, when the blood curves are given. The attenuation of the signal in the myocardial factor image in this study with the bolus injection is lower than that reported previously for infusion (*6*). This is due to the S/N ratio being proportional to the sine of the angle between the scaled variate and the covariate space (*6*). This angle is higher with the bolus because the shapes of the blood and myocardial curves differ from each other more than with infusion.

When compared with the alternative of factor analysis based on principal component analysis, which performs badly in the presence of high noise levels where there is a risk of total failure (*14*), the present method is robust. The loss due to the use of a fixed-flow model is predictable and low over a wide range of MBF values (Fig. 3). The method uses the lung curve, which has good statistics, and is devoid of myocardial spillover. The delay between the lung curve and the true arterial input function is not important when generating myocardial factor images (Table 2), as opposed to when MBF is calculated (*15*).

TABLE 1
Comparison of Results Using Factor Images and Washout Images

Input	ROIs	MBF [ml min^{-1} ml^{-1}]	TF [ml ml^{-1}]	$V_{a,total}$ [ml ml^{-1}]	$V_{a,rvc}$ [ml ml^{-1}]
LVC	Septum	−0.02 ± 0.06	−0.02 ± 0.02†	0.05 ± 0.04‡	0.03 ± 0.06
	Nonseptum	0.01 ± 0.06	0.01 ± 0.02	0.06 ± 0.03‡	
LA	Septum	−0.03 ± 0.08	−0.02 ± 0.03*	0.04 ± 0.03†	0.02 ± 0.05
	Nonseptum	0.01 ± 0.08	0.00 ± 0.03	0.05 ± 0.03†	

*$p \leq 0.05$.
†$p \leq 0.01$.
‡$p \leq 0.001$.

ROIs = regions of interest; MBF = myocardial blood flow; TF = tissue fraction; LVC = left ventricular cavity; LA = left atrial.

Average difference (± s.d.) of MBF, TF, total spillover ($V_{a,total}$) and spillover from the right ventricular cavity ($V_{a,rvc}$) when the ROIs are defined on factor images and on traditional images (washout, extravascular density and $C^{15}O$ blood volume images) using LVC and LA input curves. Paired t-test, degrees of freedom = 14 for LVC and degrees of freedom = 11 for LA.

TABLE 2
Retrieval of Signals in Myocardial Factor Images

Model	Myo	Myo + 5 sec	Myo + 10 sec	RVC blood	LVC blood
Lung ± 10 sec	0.57 ± 0.03	0.61 ± 0.03	0.65 ± 0.04	−0.01 ± 0.05	−0.04 ± 0.05
Lung ± 5 sec	0.61 ± 0.04	0.65 ± 0.04	0.69 ± 0.04	−0.03 ± 0.04	−0.05 ± 0.05

The average magnitude ± s.d. (from 15 subjects) of myocardial and blood signals in the myocardial factor images relative to the magnitude of the signals in optimally weighted summed images. Negative values represent oversubtractions. The magnitude of myocardium (Myo, Myo+5 sec, Myo+10 sec) depends on the actual delay and dispersion between the lung and the coronary arteries (0 sec, 5 sec and 10 sec). It was assumed that MBF = 0.75 ml min^{-1} ml^{-1}. The covariate factors (x_{lvc}, x_{rvc}) were modeled as lung−Δt and lung+Δt where Δt = 10 sec (5 sec).

RVC = right ventricular cavity; LVC = left ventricular cavity.

The average delay through the lungs is the lung water content (about 0.5–1 l) divided by cardiac output (about 6 l/min), giving a delay of about 5–10 sec. In cases with increased lung water content (like pulmonary edema) and/or reduced cardiac output, the delay will increase. This could result in a poorer subtraction of the blood from the heart cavities if the actual delay through the lung were significantly larger than the model value (2Δt, i.e., 10 sec and 20 sec in this study). In these situations, Δt could be increased. The used delay values (±Δt) were chosen to give good blood subtraction for most clinical patients.

Dispersion will result in a mixture of delayed TACs. The retrieval of the myocardial signal will, therefore, be a corresponding mixture of retrievals of delayed, but not dispersed, TACs. This effect of dispersion is modest (see Table 2). Another effect of dispersion is the widening of the blood TACs. This will result in a slightly lower retrieval of the myocardial TACs, but even when the blood curves are about 90 sec wide, the retrieved myocardial signal is sufficiently high (*6*). Further studies will be required to assess the effect on the factor images of increased delay and dispersion through the lung.

Patient movement during a dynamic scan is an important problem with factor analysis using principal component analysis. The extracted factor curves may be wrong, and the factor images may be meaningless. The factor curves are less affected in the present method because they are based on the lung curve, which is insensitive to movement as long as the ROIs are kept at a safe distance from the chest wall and from the heart. If the factor curves are correct, then the effect of movement is less severe. Movement may then create (positive or negative) shadows around the edges of the anatomical structures. In contrast to the principal component analysis, the present method allows calculation of the amplitude of the myocardium as a function of different MBF values (the projected variate curve in Fig. 3). Over a wide range of normal baseline MBF values, the amplitude does not vary substantially. The myocardial factor images, therefore, essentially represent myocardial tissue density images for baseline flow. With very low flow, the amplitude falls so that scar tissue, with very low flow, should appear faint. Figure 3 also shows that myocardial images with hyperemic MBF will appear with a reduced S/N ratio. Although to a lesser degree, this also happens for theoretically optimal factor images (total signal − covariates). When creating factor images with hyperemic MBF, the modeled myocardial factor curve could use an MBF value higher than 0.75 ml min^{-1} ml^{-1}. However, this is usually not necessary, because, in most cases, a baseline MBF study is also performed and this can be used for ROI definition.

Factor analysis, including principal component analysis, has been applied successfully to cardiac PET studies with good S/N ratios like $^{13}NH_3$ (*16*) and fluorodeoxyglucose (*17*). Factor analysis has also been applied to animal $H_2{}^{15}O$ studies where it may produce MBF images (*18*). The latter studies obtained linearity for low-to-normal MBF by restricting the duration of the scan, so that the factor images were essentially first-pass extraction images. The extraction of the factors requires a short bolus, which makes the blood and the myocardial factor TACs more distinct. In this study, the aim was to develop a robust method for generating images of the heart in (potentially noisy) patient studies. A relatively wide bolus was used to avoid too much detector dead time. While accepting nonlinearity for normal and high flows (Fig. 3), the duration of the scan was increased to obtain best possible statistics.

Figure 3 illustrates that the signal-to-noise ratio in the myocardial factor images is approximately 60% of that in the optimally weighted (*6*) summed images. The factor images may, therefore, contain more noise than the washout images. Since even filtered backprojected washout images sometimes contain an unacceptable level of noise, it is obvious that iterative reconstruction (*10*) is needed with the factor images to reduce noise. It is of interest to note that the generation of myocardial factor images using linear dimension reduction in a less general form was first suggested in 1989 (*19*). At that time, however, the proposed method could not be implemented for routine use simply because of high noise levels due to the lack of iterative reconstruction techniques and the use of prolonged $C^{15}O_2$ inhalation (smaller angles between the variate and the covariate spaces).

The main weakness of the present method is the simple modeling of the LVC and the RVC curves as the lung curve ± 5 sec or ± 10 sec, resulting in slight oversubtraction of blood in the myocardial factor images (Table 2). More importantly, however, MBF values are unaffected (Table 1). It should be noted that it is possible to eliminate this error in blood subtraction by using the present factor images to define ROIs for the LVC and RVC. In a second iteration, the measured LVC and RVC time-activity curves could then be used instead of the modeled ones to generate a new set of factor images. These curves contain, however, spillover of myocardial activity and more noise. Further studies are required to evaluate this approach.

A practical drawback of the proposed method is the increased processing time. The traditional analysis of two dynamic scans without iterative reconstruction takes about 1 hr (not counting the time for filtered backprojection). The proposed method requires iterative reconstruction of factor images, which adds 10 hr processing time without user intervention on a SUN SPARC (Sun Microsystems, Inc., Palo Alto, CA) 20 with one 150 MHz HyperSparc CPU. The iterative reconstruction could, however, be reduced to 1½ hr if 32 iterations, and four subsets (*20*) were used.

CONCLUSION

This study shows that it is possible to generate myocardial images directly from a dynamic $H_2{}^{15}O$ study without the need for a $C^{15}O$ scan. These images can be used for ROI definition. Use of these ROIs provides essentially the same MBF and TF values as when the ROI definition is based on the $C^{15}O$ scan. The elimination of $C^{15}O$ has several advantages: (a) the radiation dose to the patient is substantially reduced (~50%); (b) no gas delivery system and control are required; (c) the study duration is reduced by about 15 min; and (d) the chance of movement artifacts is reduced.

The present method of generating myocardial factor images is robust and results in nearly optimal S/N ratios in the factor images. It has several advantages over traditional factor analysis. It uses a low noise lung curve for modeling the factor curves and determining the final oblique rotation, and it does not use principal component analysis, which is sensitive to noise in the data.

ACKNOWLEDGMENTS

The authors would like to thank professors Terry Jones and Sandy McNeish, together with the staff of the Cyclotron Unit, for their interest and support.

REFERENCES

1. Bergmann SR, Herrero P, Markham J, Weinheimer CJ, Walsh MN. Noninvasive quantitation of myocardial blood flow in human subjects with oxygen-15-labeled water and PET. *J Am Coll Cardiol* 1989;14:639–652.
2. Araujo LI, Lammertsma AA, Rhodes CG, et al. Noninvasive quantification of regional myocardial blood flow in coronary artery disease with oxygen-15-labeled carbon dioxide inhalation and PET. *Circulation* 1991;83:875–885.
3. Lammertsma AA, De Silva R, Araujo LI, Jones T. Measurement of regional myocardial blood flow using $^{15}C\ ^{2}O$ and PET: comparison of tracer models. *Clin Phys Physiol Meas* 1992;13:1–20.
4. Rhodes CG, Wollmer P, Fazio F, Jones T. Quantitative measurement of regional extravascular lung density using positron emission and transmission tomography. *J Comput Assist Tomogr* 1981;5:783–791.
5. Hermansen F, Lammertsma AA. Linear dimension reduction of sequences of medical images: I. optimal inner products. *Phys Med Biol* 1995;40:1909–1920.
6. Hermansen F, Bloomfield PM, Ashburner J, Camici PG, Lammertsma AA. Linear dimension reduction of sequences of medical images: II. direct sum decomposition. *Phys Med Biol* 1995;40:1921–1941.
7. Hoffman EJ, van der Stee M, Ricci AR, Phelps ME. Prospects for both precision and accuracy in PET. *Ann Neurol* 1984;15(suppl):S25–34.
8. Hermansen F, Rosen SD, Fath-Ordoubadi F, et al. Measurement of myocardial blood flow with oxygen-15 labelled water: comparison of different administration protocols. *Eur J Nucl Med* 1998;25:751–759.
9. Hermansen F, Spinks TJ, Camici PG, Lammertsma AA. Calculation of single detector efficiencies and extension of the normalization sinogram in PET. *Phys Med Biol* 1997;42:1143–1154.
10. Shepp LA, Vardi Y. Maximum likelihood reconstruction for emission tomography. *IEEE Trans Med Imaging* 1982;MI-1:113–122.
11. Lange K, Carson R. EM reconstruction algorithms for emission and transmission tomography. *J Comput Assist Tomogr* 1984;8:306–316.
12. Silverman BW, Jones MC, Wilson JD, Nychka DW. A smoothed EM approach to indirect estimation problems, with particular reference to stereology and emission tomography. *J R Statist Soc B* 1990;52:271–324.
13. Iida H, Rhodes CG, de Silva R, et al. Use of the left ventricular time-activity curve as a noninvasive input function in dynamic oxygen-15-water PET. *J Nucl Med* 1992;33:1669–1677.
14. Hermansen F, Lammertsma AA. Linear dimension reduction of sequences of medical images: III. factor analysis in signal space. *Phys Med Biol* 1996;41:1469–1481.
15. Herrero P, Hartman JJ, Senneff MJ, Bergmann SR. Effects of time discrepancies between input and myocardial time-activity curves on estimates of regional myocardial perfusion with PET. *J Nucl Med* 1994;35:558–566.
16. Wu HM, Hoh CK, Buxton DB, et al. Quantification of myocardial blood flow using dynamic nitrogen-13-ammonia PET studies and factor analysis of dynamic structures. *J Nucl Med* 1995;36:2087–2093.
17. Wu HM, Hoh CK, Choi Y, et al. Factor analysis for extraction of blood time-activity curves in dynamic FDG PET studies. *J Nucl Med* 1995;36:1714–1722.
18. Jamal F, Janier MF, Herrero P, et al. Myocardial perfusion assessment with oxygen-15-water using factor analysis [Abstract]. *J Nucl Med* 1996;37:147P.
19. Hermansen F, Lammertsma AA, Araujo L, Bloomfield P, Jones T, Lassen NA. A method to outline the myocardium in studies with a single diffusible tracer [Abstract]. *J Nucl Med* 1989:775–776.
20. Hudson HM, Larkin SL. Accelerated image reconstruction using ordered subsets of projection data. *IEEE Trans Med Imaging* 1994;20:100–108.